Materials and Design 197 (2021) 109217

Contents lists available at ScienceDirect

Materials and Design

journal homepage: www.elsevier.com/locate/matdes

Assessing the scale contributing factors of three carbide-free bainitic steels: A complementary theoretical and experimental approach

Adriana Eres-Castellanos [a], Javier Hidalgo [b], Muftah Zorgani [c], Mohammad Jahazi [c], Isaac Toda-Caraballo [a], Francisca G. Caballero [a], Carlos Garcia-Mateo [a,*]

[a] National Center for Metallugical Research (CENIM-CSIC), Avda. Gregorio del Amo 8, Madrid 28040, Spain
[b] Delft University of Technology, Materials Science and Engineering, Mekelweg 5, Delft 2628, Netherlands
[c] École de Technologie Supérieure (ETS), Mechanical Engineering, Notre-Dame Street West, Montreal 1100, Canada

HIGHLIGHTS

- Thermomechanical treatments were designed to obtain similar microstructures in terms of bainitic ferrite plate thickness
- Significant differences have been found among the microstructures, even though they were designed to be similar
- Results indicate that there might be other factors that take part in the scale of bainitic microstructures

GRAPHICAL ABSTRACT

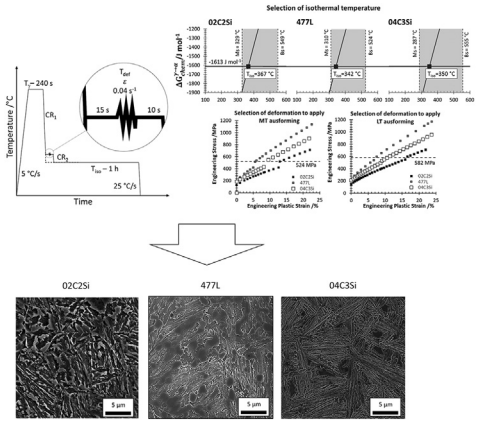

ARTICLE INFO

Article history:
Received 8 September 2020
Received in revised form 1 October 2020
Accepted 8 October 2020
Available online 10 October 2020

Keywords:
Bainite
Thermomechanical treatment
Ausforming
Microstructural characterization
Dilatometry
Anisotropy

ABSTRACT

The bainitic ferrite plate thickness is the main parameter that controls the strength of this type of microstructures. Such thickness has been proved to mainly depend on the austenite yield strength, the driving force for the transformation and the transformation temperature. However, no research has focused on how these parameters evolve throughout the transformation and how this evolution can affect the outcome. In this study, thermal and thermomechanical treatments have been performed in three selected steels. The treatments have been designed in such a way that all the mentioned parameters are comparable, aiming to obtain similar microstructures in terms of bainitic ferrite plate thickness. However, significant differences have been found among the microstructures, with variations in plate thickness larger than 100 nm. These results indicate that there might be other factors that take part in the scale of bainitic microstructures. To explain these differences and based on the kinetics of the transformation and on the carbon content of austenite at the end of the transformation, a possible explanation has been proposed.

1. Introduction

Extensive works have focused on creating a unified theory that describes how the bainitic transformation takes place, anticipating the final microstructure and properties [1–4]. Among others, many

* Corresponding author at: Av. Gregorio del Amo 8, Madrid 28040, Spain.
E-mail address: cgm@cenim.csic.es (C. Garcia-Mateo).

https://doi.org/10.1016/j.matdes.2020.109217

have studied the factors that influence the thickness of the bainitic ferrite (α) plates [5,6], a key factor to improve the strength of the final microstructure [1–4].

Several factors have been identified to be relevant for the bainitic ferrite plate thickness. The austenite (γ) yield strength at the transformation temperature, YS_{Tiso}, has been suggested to be the most important factor among them [5–8]. This is because the shape deformation associated with the bainitic transformation is plastically accommodated by the austenite phase [9]. Accordingly, a high YS_{Tiso} would prevent the bainitic ferrite/austenite interphase from moving freely, which would decrease the thickness of the formed bainitic ferrite plate. The YS_{Tiso} has been commonly adjusted by changing the transformation temperature [10], although more recent works have modified it by work hardening prior to the transformation during the thermomechanical treatment of ausforming [7,11,12].

The impingement events also influence the size of the bainitic plates [13]. Such events are mainly dependent on the Prior Austenite Grain Size (PAGS) [14] and on the driving force for the transformation of austenite into ferrite, $\Delta G^{\gamma\rightarrow\alpha}$ [6]. Although, the PAGS mainly affects the length of the bainitic plates [14], it may also modify their thickness [15–17]. Regarding $\Delta G^{\gamma\rightarrow\alpha}$, it affects the transformation rate, which in turn influences therefore the number of impingement events and the bainitic ferrite plates thickness [5–7,18].

Lastly, the isothermal holding temperature, T_{iso}, plays a minor role on the plate thickness. Although it importantly influences the YS_{Tiso} and $\Delta G^{\gamma\rightarrow\alpha}$ [5,8], once these two effects are taken out of the equation, the only effect that the temperature could have on the plate thickness would be also related to dynamic recovery effects. However, the impact of such effects on the thickness of the bainitic plates has been found to be negligible for temperatures in the range 260–460 °C [5].

Although the above parameters (YS_{Tiso}, $\Delta G^{\gamma\rightarrow\alpha}$ and T_{iso}) have been linked to the final scale of the bainitic microstructures, no research has been focused on how they evolve with respect to time throughout the transformation and how such evolution could alter the overall bainitic ferrite plate thickness. In this study, with the aim to acknowledge whether a further research is required, three selected steels were subjected to different thermal and thermomechanical treatments resulting in bainitic microstructures. The process parameters were selected in such a way that YS_{Tiso}, PAGS, $\Delta G^{\gamma\rightarrow\alpha}$ and T_{iso} are similar in all cases, aiming to obtain similar microstructures in terms of bainitic ferrite plate thickness. In order to analyze whether the mentioned aim had been achieved, a thorough microstructural characterization was carried out, including a quantification of the plate thickness on Scanning Electron Microscopy (SEM) micrographs [19].

2. Experimental

For the present work, three different steels were used: a designed low carbon steel (02C2Si) and two medium carbon commercial steels (477 L, produced by Ovako, and 04C3Si, produced by Sidenor). Their simplified nominal chemical compositions can be found in Table 1. Note that the full nominal chemical compositions cannot be shown as they are classified. They were selected because of different reasons: a) two of them have the same C content (04C3Si and 477 L), whereas the designed steel (02C2Si) has only 0.2 wt% C; this enables to study the effect of carbon on the bainitic ferrite plate thickness; b) the sum of the Si and Mo contents (Si + Mo) is similar for two of the steels with different C contents (02C2Si and 477 L), whereas the 04C3Si steel contains a higher Si + Mo content; note that Si and Mo are the elements which play the most important role when it comes to the austenite strength besides C [20]; and c) all the steels have Si contents higher than >1.5 w.t.% to prevent carbide precipitation from austenite during the bainitic transformation [21].

Table 1
Simplified nominal steels chemical compositions, all in wt%.

Steel	C /wt%	Si + Mo /wt%	Cr + Mn /wt%
02C2Si	0.2	2.0	2.9
477 L	0.4	2.1	3.0
04C3Si	0.4	3.3	1.7

Thermal and thermomechanical treatments were performed in a Bahr 805D high-resolution dilatometer, which enables to study phase transformations by monitoring the changes in the sample length. The temperature can be increased by an induction heating coil, whereas it can be decreased by using Helium as quenching gas. K type thermocouple welded to the central part of the sample surface was used for recording temperature evolution. The dilatometry and the compression tests were performed using two different specific modules: the former tests were carried out using the basic dilatometer module, equipped with fused silica push-rods to measure longitudinal length changes, whereas the latter ones were carried out by using a deformation module, with Si_3N_4 punchers separated from the sample by Mo films in order to reduce friction and to increase the temperature homogeneity in the specimens. The mentioned punchers also enabled to measure the longitudinal length changes. Cylindrical specimens of 10 mm length and 4 mm diameter were used for pure dilatometry and specimens with 5 mm diameter were used for the deformation tests.

Among other benefits, the dilatometric data are useful to determine some critical temperatures. In this work, the Ac3 and the Ms. temperatures were determined by the offset method explained in Ref. [22]. This consists in defining the corresponding critical temperature as the temperature at which the temperature-time curve deviates by a certain value, i.e. 0.2% in our particular case, from the linearity.

In order to determine the volume fractions of retained austenite and bainitic ferrite, the technique X-ray diffraction (XRD) was used. Samples were step-scanned in a Bruker D8 Advance diffractometer with Bragg-Brentano geometry, equipped with a graphite monochromator and a Vantec position sensitive detector. The diffractometer has a rotating Co anode X-ray tube as a radiation source and its current and voltage were, respectively, 35 mA and 45 kV. The measurements were made by a coupled Θ-2Θ scan in the range 30–130°, with a step size of 0.026° and a counting time per step of 2 s. Austenite fraction was calculated by comparing the areas under the ferrite peaks {110}, {200}, {211} and {220} with the areas under the austenite peaks {111}, {200}, {220} and {311}, assuming that the sample consists of only two phases [23]. Using several peaks avoids non-accurate results related to crystallographic texture [24]. The Rietveld refinement method [25] was applied to calculate the lattice parameters of both phases present in the microstructure, by using the version 4.0 of TOPAS software (Bruker AXS). The austenite lattice parameter was used to calculate the austenite carbon content by using the formula proposed by Dyson and Holmes [26].

Standard metallographic procedures were used for XRD samples preparation, followed by a final set of etching and polishing cycles in order to remove the plastically deformed layer formed on the sample surface during the grinding step. It is important to remove that layer since it might contain deformation induced martensite, not present in the original microstructure.

The microstructure was revealed by using standard metallographic procedures, followed by a final etching with a 2% or 3% Nital solution for times lying between 2 and 20 s, depending on the steel.

The different microstructures were characterized by using field emission gun scanning electron microscopy (FEG-SEM), inspecting the central part of the sample, where the local plastic strain is maximum [27,28]. Both the transverse and the longitudinal sections were observed to identify possible anisotropy effects in the development of the microstructure [29].

The plate thickness, t, was measured according to the procedure described in Ref. [19], which consists in measuring enough linear intercepts on SEM micrographs to obtain reliable statistics, i.e. at least 200

linear intercepts, and subsequently applying a stereographic correction to the mean linear intercept ($\overline{L^{\alpha}}$), $t = 2\overline{L^{\alpha}}/\pi$ with a 95% confidence error $E = \pm 1.96 \cdot \sigma_L^{\alpha}/\pi\sqrt{N}$, where σ_L^{α} symbolizes the standard deviation of the intercepts and N is the number of measurements. It is worth noting that this procedure has been proven to be accurate and in agreement with respect to using Transmission Electron Microscopy (TEM) measurements, while it is less time consuming [19]. Nonetheless, the method might not be appropriate for microstructures exhibiting anisotropy [29]. However, it can be helpful to obtain a good estimate of the microstructure refinement level if it is measured on both the transverse and the longitudinal sections. Also, note that other phases with morphologies different than plate-like, such as granular bainite, cannot be measured by this methodology. In case there were two different morphologies of bainite in a microstructure, only plate-like bainite was measured.

The Prior Austenite Grain (PAG) boundaries were revealed by thermal etching technique. The technique consists in subjecting a sample, which has to be carefully prepared as explained elsewhere [30], to the selected austenitization conditions followed by vacuum-cooling to room temperature, which enables to reveal the parent grains grooves. The PAG areas were measured on light optical micrographs by the image processing program ImageJ [31], and the equivalent diameter of the grains was calculated from them.

Vickers hardness measurements were made using an applied load of 10 kg. Three different measurements on the transverse section and three additional measurements on the longitudinal section were performed. Since no significant differences were found between measurements on both sections, the presented results correspond to the average of both of them.

Thermodynamic calculations were performed on the MTDATA software (version 4.73), which relies on the NPL-plus database for steels [32] and they were used to calculate the critical temperatures as is explained in more detail in the following section.

3. Methodology for the selection of pure isothermal and ausforming parameters

The designed treatments always started by austenitizing the samples at a temperature T_γ for 240 s. In the case of the pure isothermal treatments, this austenitization step was followed by a rapid cooling (with a cooling rate CR_1) to T_{iso}. This temperature was held for 1 h before the final cooling to room temperature took place. The dashed line in Fig. 1a illustrates the treatment, whereas the solid line corresponds to the ausforming treatments. In this case, the austenitization was followed by a cooling (also with a cooling rate CR_1) down to the deformation temperature, T_{def}. Note that in all cases $T_{def} < T_{NR}$ (non-recrystallization temperature). With the aim of completely homogenizing the sample temperature and stabilizing the system before the deformation step takes place, there must be a short holding time of 15 s right after cooling and before deformation. Subsequently, a (engineering) deformation ε was applied, by using a strain rate of 0.04 s^{-1}, and the temperature was held for 10 s to relax all the internal stresses and avoid their influence on the transformation during the isothermal step. After this short holding time, samples were cooled down to T_{iso} with a cooling rate CR_2, kept as 25 °C/s for all the experiments. Samples were finally held at T_{iso} for 1 h and cooled down to room temperature with a cooling rate of 25C/s.

The justification for the selection of T_γ, T_{iso}, CR_1, T_{def} and ε is discussed in the following text. Those parameters were selected so that $\Delta G^{\gamma\rightarrow\alpha}$, PAGS, T_{iso} and YS_{Tiso} (the last parameter, only in the case of the ausforming treatments) are similar. Fig. 2 includes a diagram where the most important criteria used for the selection of some of the processing parameters in this work are shown.

3.1. Selection of non-deformation-related processing parameters, aiming to obtain similar plate thicknesses

Firstly, the selection of T_γ and T_{iso} enables to obtain similar PAGS [14] and $\Delta G^{\gamma\rightarrow\alpha}$ [6], respectively. It was assumed that the PAGS would be approximately the same if the austenitization took place at a temperature of 30 °C above the experimentally estimated Ac3 temperature of each steel, see Table 2 for the Ac3 temperatures and Table 3 for the selected T_γ. Thermal etching proved that the assumption was correct, as the PAGS are of the same order of magnitude, with a minor variation of 16–19 μm as observed in Table 3.

Regarding T_{iso}, a thermodynamic analysis was performed to choose a specific T_{iso} for each steel so that the same chemical driving force, $\Delta G_{chem}^{\gamma\rightarrow\alpha}$, was obtained for all the treatments. $\Delta G_{chem}^{\gamma\rightarrow\alpha}$ was calculated as a function of T_{iso} for every steel as follows: $.\Delta G_{chem}^{\gamma\rightarrow\alpha} = G_{chem}^{\alpha} - G_{chem}^{\gamma}$, where G_{chem}^{α} and G_{chem}^{γ} are the free energies of α and γ, respectively, obtained using MTDATA. Fig. 3 shows the evolution of $\Delta G_{chem}^{\gamma\rightarrow\alpha}$ with respect to T_{iso}. The isothermal temperatures were selected so that they corresponded to $\Delta G_{chem}^{\gamma\rightarrow\alpha} = -1613$ J mol^{-1}, always making sure that they were between the theoretical Bs and the Ms. temperatures. The Bs temperature was considered to be the maximum temperature at which the energy balances in Eqs. (1) and (2) are met, where $\Delta G_{chem}^{\gamma\rightarrow\gamma'+\alpha}$ is the driving force for the nucleation under paraequilibrium conditions and was calculated by MTDATA, G_N is the critical driving force to stimulate the nucleation of bainitic ferrite, which can be calculated based on the method reported in [33] and G_{SB} is the stored energy of bainite, which lies in the range 200–600 J mol^{-1} [10,34,35]. Regarding the Ms. temperature, it was experimentally estimated and theoretically calculated by applying the balance in Eq. (3), where $G_N^{\alpha'}$ is the critical driving force needed to stimulate martensite by an athermal, diffusionless nucleation and growth mechanism and can be calculated as explained in Ref. [36]. See Table 2 for the values of these critical temperatures.

$$\Delta G_{chem}^{\gamma\rightarrow\gamma'+\alpha} \le G_N \tag{1}$$

$$\Delta G_{chem}^{\gamma\rightarrow\alpha} \le G_{SB} \tag{2}$$

$$\Delta G_{chem}^{\gamma\rightarrow\alpha} \le G_N^{\alpha\prime} \tag{3}$$

All the mentioned T_{iso} are included in Table 3. Note that these temperatures are very close to each other, i.e. the maximum difference among them is 25 °C, which is expected to have a negligible effect due to recovery phenomena.

For the consistency of the methodology proposed in this work and in order to avoid adding variables that could jeopardize the design of other treatment parameters [38,39], it is essential that the isothermal step (in the case of the pure isothermal treatments) and the deformation step (for the ausforming treatments) begin from a 100% austenitic microstructure. Thus, it is necessary to select CR_1 so that the corresponding cooling step is fast enough to avoid any phase transformation, especially reconstructive transformations, prior to the mentioned steps. The selection of the CR_1 was based on Continuous Cooling Transformation Diagrams, which showed that the selected values led to fast enough cooling steps to prevent the mentioned phases from forming.

3.2. Selection of deformation-related processing parameters, aiming to obtain similar plate thicknesses

As previously mentioned, the most important parameter related to the plate thickness is the YS_{Tiso}. Varying T_{iso} in pure isothermal treatments only enables to fix either $\Delta G_{chem}^{\gamma\rightarrow\alpha}$ or YS_{Tiso} and, therefore, the isothermal treatments of this study are characterized by having different YS_{Tiso} values. To obtain such values, single hit compression tests were carried out, as indicated in Fig. 1b, where $T_{def} = T_{iso}$, i.e. samples were

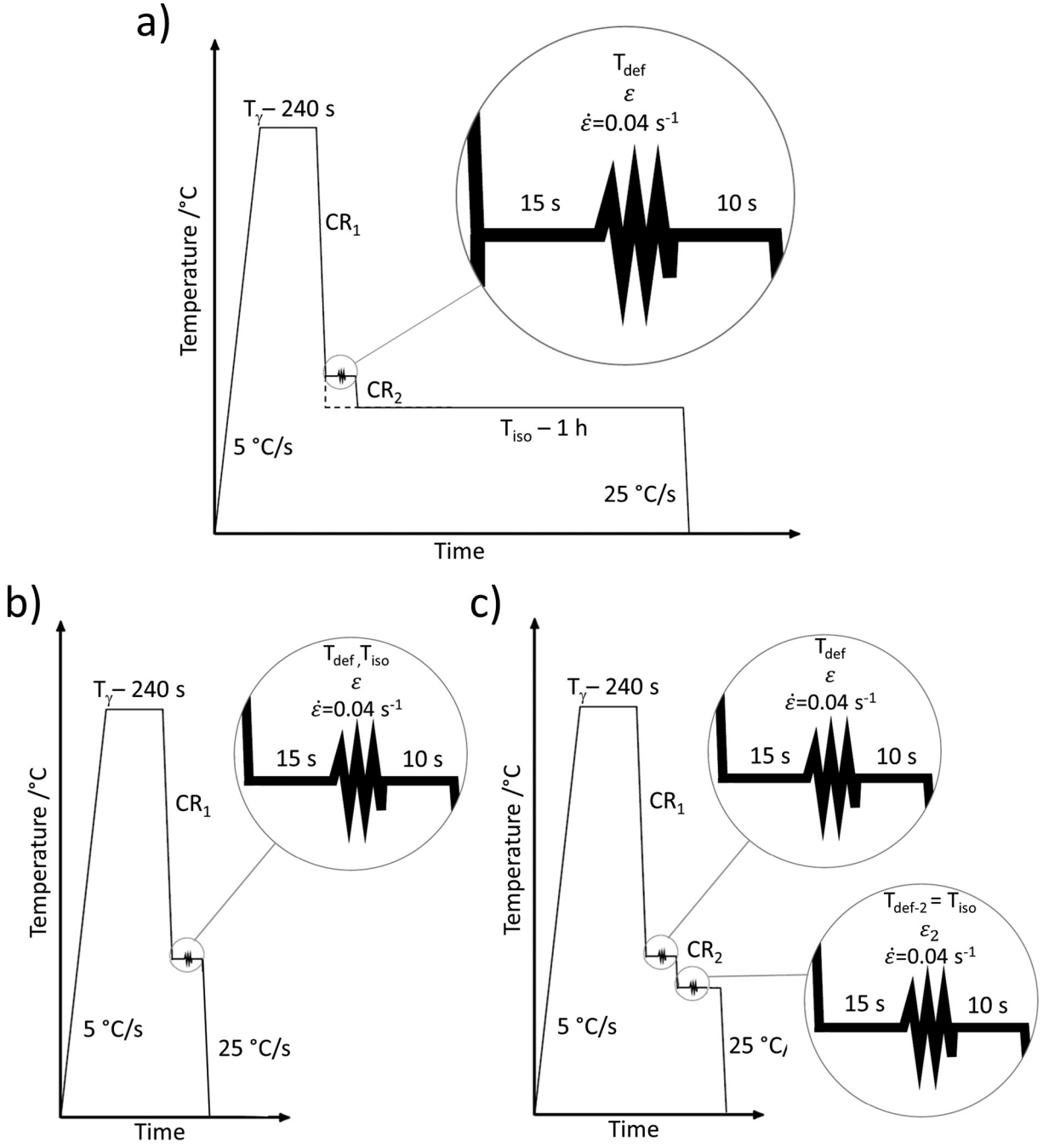

Fig. 1. a) Scheme of thermal and thermomechanical treatments characterized in this study. The dashed line and the solid lines correspond to the pure isothermal treatment and to the ausforming treatments, respectively; b,c) Performed treatment to obtain high temperature stress-strain curves and to estimate the yield strength at the isothermal (b) or the deformation (c) temperature. T_γ, T_{def} and T_{iso} stand for austenitization, deformation and isothermal temperatures, respectively, whereas CR_1 and CR_2 are the cooling rates of the incated steps. ε and ε_2 are the strains applied during the first and the second deformation steps.

deformed at the same temperatures that they would be isothermally treated in the pure isothermal treatments in Fig. 1a. After full austenitization, specimens were cooled down to the deformation temperature and deformed up to the dilatometer load cell limit. The proof stress values were estimated by the 0.2% offset criterion and are included in Table 3. Note that these values were assumed to be a good approximation of YS_{Tiso}, as curves did not show a clear yield point. Also note that, although the YS_{Tiso} values obtained for the two medium carbon steels are rather similar, this condition is not met for the low carbon steel. Therefore, ausforming treatments will be required to do so.

During the ausforming treatments, if austenite is deformed prior to the bainitic transformation, YS_{Tiso} can be tailored. However, the driving force for the transformation is then altered, as the total driving force for the transformation is $\Delta G^{\gamma\rightarrow\alpha} \leq \Delta G_{SB} - \Delta G_{disl}$, where ΔG_{disl} is the additional driving force needed so that the interface overcomes the dislocation density introduced by the plastic deformation [40–42]. ΔG_{disl} depends on the dislocation density introduced at T_{def} – which is mainly related to the maximum achieved stress at that temperature, σ_{max} (T_{def}), [43] - and on several parameters that are a function of T_{iso} [40–42]. Hence, the deformation steps of the ausforming treatments were selected so that YS_{Tiso} is the same for all three steels, being σ_{max} (T_{def}) as close as possible. In that way, the four parameters (PAGS, $\Delta G^{\gamma\rightarrow\alpha}$, YS_{Tiso} and T_{iso}) would be similar for the three steels. In this study, for every steel, two different thermomechanical treatments

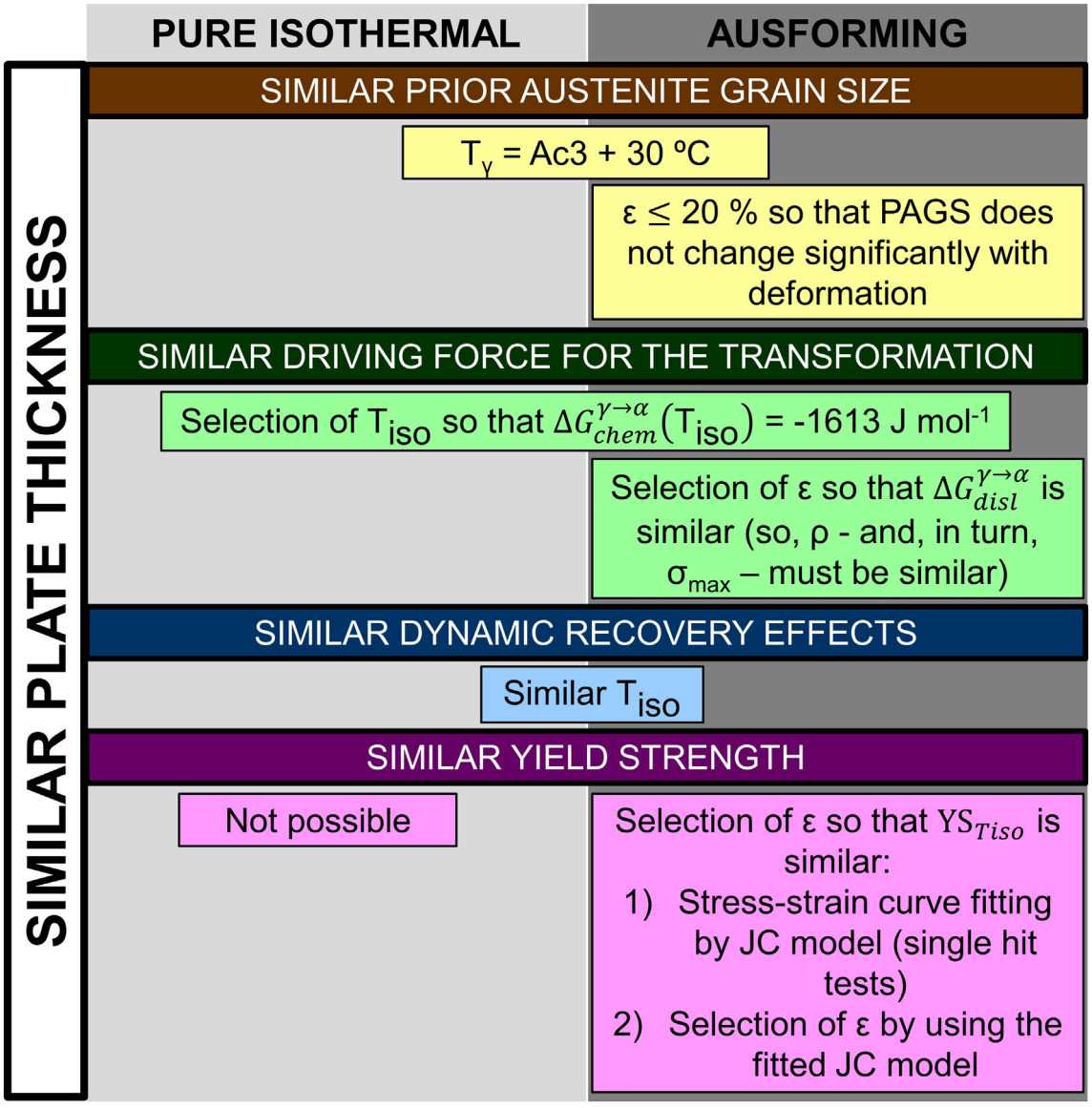

Fig. 2. Schematic diagram where the criteria used to select some of the processing parameters in this work are shown.

were performed, each of them characterized by a different T_{def}, correspondent to either a medium (MT) or a low temperature (LT) ausforming treatment, according to Ref. [29]. Such deformation temperatures are 170 and 50 °C above the isothermal temperature, respectively, see Table 3. Temperatures were selected in that way so that all the MT T_{def} were close to the theoretical Bs temperature and all the LT T_{def} were below the theoretical Bs temperature.

3.2.1. Proposing a method for the determination of the austenite yield strength of 04C3Si steel: An experimental and theoretical approach

The selection of the applied strain is subsequently discussed. As the goal of this step is to obtain similar values of YS_{Tiso} for the three steels, it has to be reminded that the yield strength varies due to both, the work hardening because of the applied deformation and the temperature decrease from T_{def} to T_{iso}. The problem must be thus divided into different parts: (1) estimating the yield strength before deformation takes place,

Table 2
Steels critical temperatures, where the Ac3 and Ms. temperatures on the left have been experimentally estimated, whereas the critical temperatures on the right have been calculated according to Ref. [37]. The calculation of the temperatures Ms.(σ), Md*, Bs(σ) and Bd* will be regarded in Section 3.2.4.

Steel	Experimental results		Theoretical results					
	Ac3 /°C	Ms / °C	Ms / °C	Ms(σ) / °C	Md* / °C	Bs / °C	Bs(σ) / °C	Bd* / °C
02C2Si	870	329	327	342 ± 3	376 ± 9	549	549	≤643 ± 47
477 L	936	310	283	300 ± 3	365 ± 14	524	524	≤667 ± 51
04C3Si	961	287	279	302 ± 3	349 ± 12	555 ± 42	584 ± 36	666 ± 53

Table 3
Selected thermal and thermomechanical parameters and values of all the parameters that affect the plate thickness for each steel and treatment.

Steel	T_γ /°C	CR_1 /°C/ s	T_{iso} /°C	T_{def} /°C	ε /%	PAGS /μm	$\Delta G^{\gamma\to\alpha}_{chem}$ /J mol^{-1}	Estimated YS_{Tiso} /MPa	Predicted YS_{Tiso} /MPa	σ_{max} (T_{def}) /MPa	ρ /m^{-2}	ΔG_{disl} /J mol^{-1}
02C2Si	900	30	367	–	–	19 ± 1	−1613	145	145	–	10^{11}	–
				530	16.0			535	524	428	$2.19\cdot10^{14}$	119
				410	20.0			701	582	562	$4.76\cdot10^{14}$	177
477 L	965	20	342	–	–	16 ± 2		206	206	–	10^{11}	–
				512	8.5			560	524	437	$1.51\cdot10^{14}$	97
				392	10.5			597	582	568	$3.70\cdot10^{14}$	154
04C3Si	990	15	350	–	–	18 ± 2		220	220	–	10^{11}	–
				520	10.0			544	524	435	$1.29\cdot10^{14}$	90
				400	10.0			723	582	497	$2.15\cdot10^{14}$	117

$YS_{Tdef\text{-}bef}$; (2) estimating the yield strength after a certain deformation ε has been applied, $YS_{Tdef\text{-}after} = f(\varepsilon)$, and estimating the yield strength increase because of work hardening (ΔYS_{WH}, see Eq. (4)) and (5) studying how much the yield strength increases when decreasing the temperature from T_{def} down to T_{iso} ($\Delta YS_{Tdef\text{-}Tiso}$, Eq. (5)).

$$\Delta YS_{WH} = YS_{Tdef-after} - YS_{Tdef-bef} \quad (4)$$

$$\Delta YS_{Tdef-Tiso} = YS_{Tiso} - YS_{Tdef-after} \quad (5)$$

Hence, the YS_{Tiso} is the summation of $YS_{Tdef\text{-}bef}$, ΔYS_{WH} and $\Delta YS_{Tdef\text{-}Tiso}$, see Eq. (6):

$$YS_{Tiso} = YS_{Tdef-bef} + \Delta YS_{WH} + \Delta YS_{Tdef-Tiso} \quad (6)$$

For a given ausforming treatment and a strain ε, the above three terms can be obtained by a thermomechanical treatment consisting of an austenitization step, followed by two deformation steps at T_{def} and T_{iso}, as depicted in Fig. 1c. By carrying out that thermomechanical treatment, two stress-strain curves can be obtained, as shown in Fig. 4, and from them, $YS_{Tdef\text{-}bef}$ and YS_{Tiso} can be estimated by using the 0.2% offset criterion – note that, again, the proof strength were assumed to be a good approximation of the yield strengths -. $YS_{Tdef\text{-}after}$ can be assumed to be the maximum stress during the first deformation step and ΔYS_{WH} and $\Delta YS_{Tdef\text{-}Tiso}$ can then be calculated as per Eqs. (4,5).

The aimed YS_{Tiso} was determined using double hit compression tests for the 04C3Si steel (Fig. 1c) where ε at T_{def} is always 10% (high enough to plastically deform the austenite) and the value of ε_2 at T_{iso} is not relevant, provided that the stresses reached are high enough to measure the yield strength at such temperature. The obtained values are included in Table 3 and the stress-plastic strain curves can be found in Fig. 5. It is clear that the double hit tests with T_{def} = 400 °C presented a fast strengthening right after the second deformation started, as seen in Fig. 5b. This suggested that other stronger secondary phases were present, apart from austenite, in accordance with previous studies on stress and strain induced transformations [37,44–48].

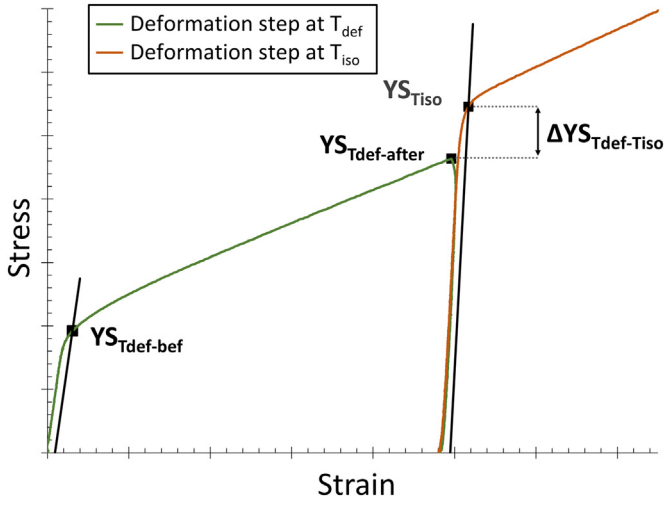

Fig. 4. Illustration of the stress strain curves obtained after performing the thermomechanical treatment depicted Fig. 1c, where $YS_{Tdef\text{-}bef}$, $YS_{Tdef\text{-}after}$ and YS_{Tiso} stand for the yield strengths of the austenite at the T_{def} before any deformation, at T_{def} after a strain ε has been applied and at T_{iso} in ausforming treatments, respectively. $\Delta YS_{Tdef\text{-}Tiso}$ is the increase of yield strength due to the temperature drop from the deformation temperature to the isothermal one. Stress and strain are in arbitrary units.

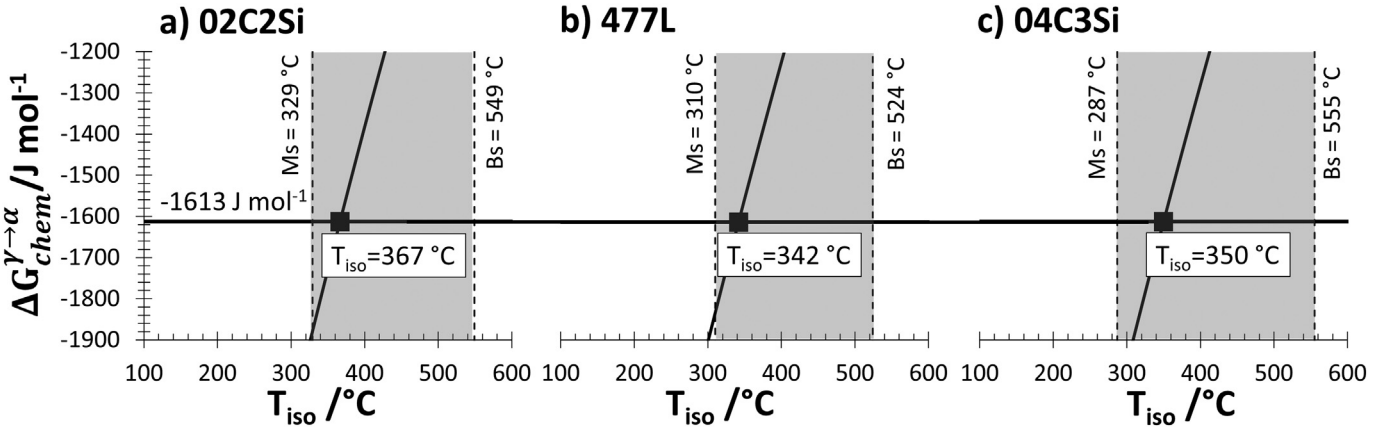

Fig. 3. Chemical driving force for the transformation to ferrite from austenite, $\Delta G^{\gamma\to\alpha}_{chem}$, as a function of the temperature (T_{iso}). The vertical dashed lines represent the experimental Martensite Start Temperature, Ms., and the theoretical Bainite Start Temperature, Bs, delimiting the bainitic region, gray shadowed. The black square is isothermal temperature T_{iso} for which the driving force is $\Delta G^{\gamma\to\alpha}_{chem} = -1613$ J mol^{-1}.

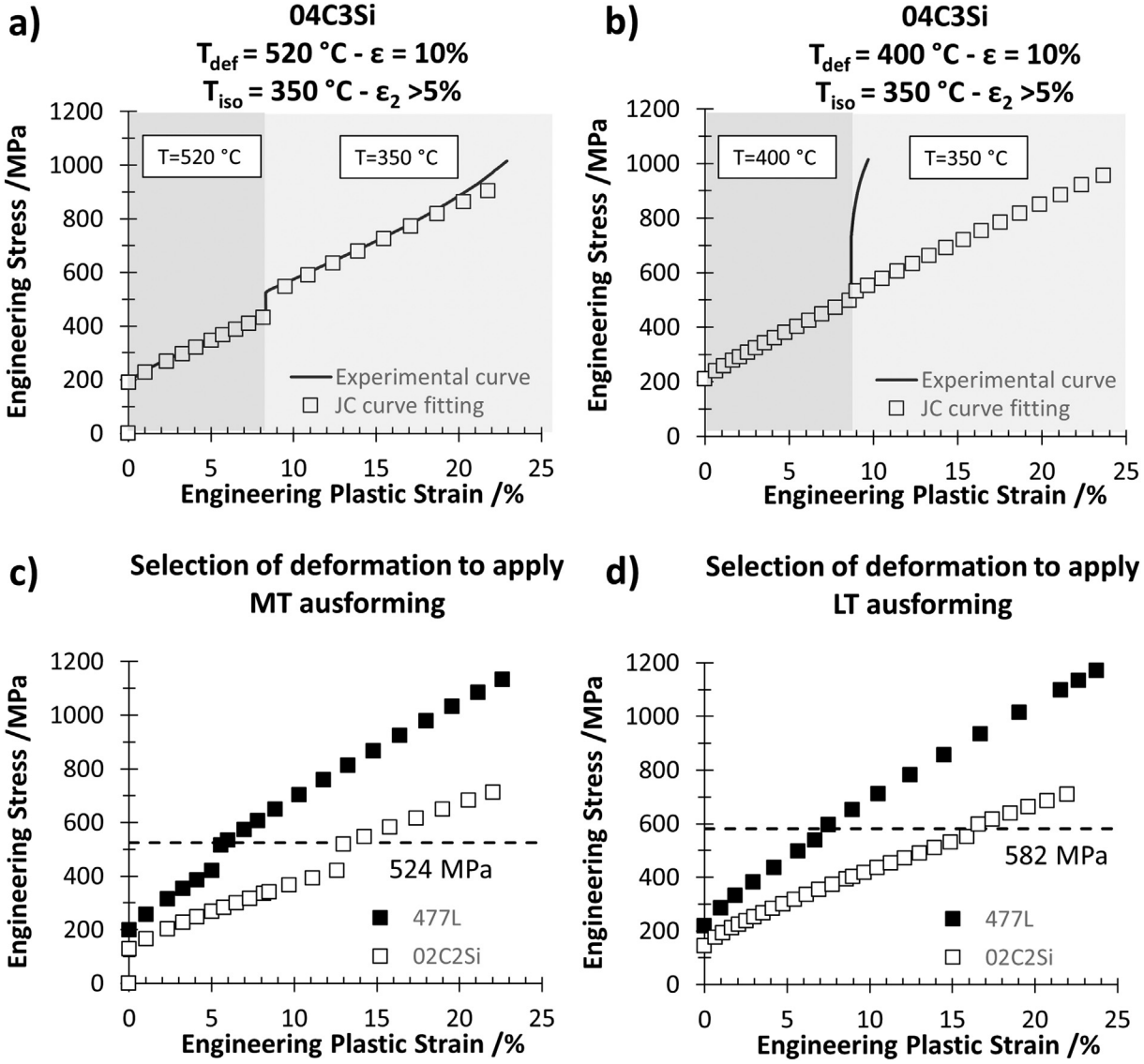

Fig. 5. a–b) Comparison of the stress-plastic strain curves obtained by the JC model with respect to the obtained experimentally (Fig. 1c) in the 04C3Si steel, for the two chosen T_{def} and ε: a) 520 °C and 10% strain; b) 400 °C and 10% strain. In both cases the T_{def-2} is 350 °C and $ε_2$ is high enough to reach the YS (>5%); c–d) Illustration showing the JC model stress-plastic strain curves used to calculate the proper value of ε: c) MT ausforming and d) LT ausforming.

To consider the possibility of strain induced transformations during the deformation steps, the stress-strain curves were calculated by the Johnson-Cook (JC) model [49]. The JC model enables to predict the flow behavior of any alloy deformed under a given strain rate $\dot{\varepsilon}_p$ and at a given deformation temperature T_{def}, once the stress-strain curve at a reference strain rate $\dot{\varepsilon}_{p0}$ - always quasi-static in order to obtain a good fitting [50] - and at room temperature T_r is known:

$$\sigma = \left(A + B \cdot \varepsilon_p^n\right) \cdot \left(1 + C \cdot \ln\left(\frac{\dot{\varepsilon}_p}{\dot{\varepsilon}_{p0}}\right)\right) \cdot \left(1 - \left(\frac{T_{def} - T_r}{T_m - T_r}\right)^m\right) \quad (7)$$

where ε_p is the unitary plastic strain, σ is the stress, T_r and T_m are the room and the melting temperatures respectively and A, B, C, n and m are the model parameters. Whereas the curve at $T_{def} = T_r$ and under $\dot{\varepsilon}_p = \dot{\varepsilon}_{p0}$ can be described by $(A + B \cdot \varepsilon_p^n)$, the effect of the temperature and the strain rate on the curve is evaluated by m and C, respectively. The JC model was originally proposed to predict the stress behavior for metals subjected to large ε_p under high $\dot{\varepsilon}_p$ and at high T_{def}. However, it can also be applied for materials in which the hardening behavior does not change significantly with $\dot{\varepsilon}_p$, such as aluminum or steel [51]. In addition to this, since a constant strain rate was used in the present work, if $\dot{\varepsilon}_{p0}$ is set as $\dot{\varepsilon}_p$, the term $\left(1 + C \cdot \ln\left(\frac{\dot{\varepsilon}_p}{\dot{\varepsilon}_{p0}}\right)\right)$ becomes equal to unity and it is not necessary to fit the constant C. Therefore, knowing the stress-strain curve at a given temperature at which no transformation is expected and the yield strengths at several temperatures, it is possible to predict the stress behavior at any other temperature as long as all the material parameters are known.

Single hit compression tests such as the ones previously described (Fig. 1b) were carried out, although in this case the T_{def} equaled the deformation temperatures selected for the ausforming treatments, see Fig. 6c for the curves. The parameters A and m can be obtained by fitting the yield strength values at different T_{def}. All yield strengths for this fitting were estimated by the 0.2% offset criterion. Once A and m are known, B and n can be determined by fitting a stress-strain curve in which no deviations associated to strain assisted transformations are observed (the one at 520 °C up to a 20% strain). Further details regarding the application of the JC model can be found in reference [52] and Table 4 includes the JC model parameters employed for the 04C3Si steel.

The stress-plastic strain curves of the 04C3Si steel can be found in Fig. 6c, where it is clear that from a plastic strain close to 12%, the JC

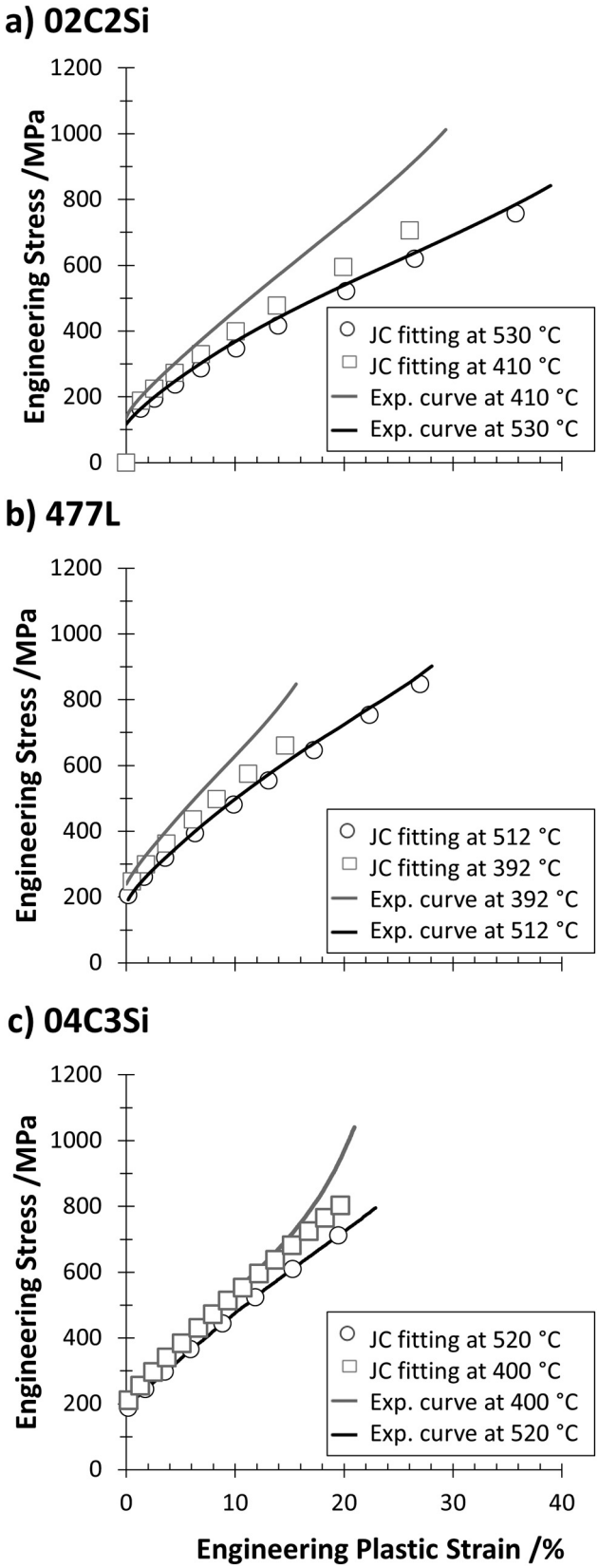

Fig. 6. Stress-plastic strain curves obtained experimentally (Fig. 1b), compared to the results obtained by the JC model, represented by either squares or circles, depending on the deformation temperature.

curve obtained for the lowest temperature, 400 °C, no longer fits the experimental one. This is most probably because a strain induced transformation is taking place, as previously reported elsewhere [37]. Strain induced bainite is harder than austenite so, since the moment when some bainite is formed, the hardening coefficient of the system increases. This is shown by a deflection in the curve. Because the JC model has been fitted with a whole austenitic system, it cannot fit the curve when there are other phases apart from austenite involved.

As the presence of phases transformed during the compression step modifies the stress-strain curves, a combination of both the experimental results and the JC model was used to assess the estimation of YS_{Tiso}. Note that it has been proven that the presence of strain induced phases could vary the average plate thickness and the hardness of microstructures obtained by ausforming treatments [37], which could alter the results given by the study.

Once the JC model was fitted, it was used to calculate the YS_{Tiso} for the LT ausforming performed on the 04C3Si steel, without the interference of strain induced phases. So far, the JC model has not succeeded to fit experimental data from sequential loading experimental data [51,53]. However, it has only been applied to predict experiments in which temperature changed gradually [53]. The current case is different, though, as the temperature change occurs 10 s after the sample has been unloaded. In addition, there is a 15 s inter-pass time before the sample is deformed again. In this way, it is made sure that the sample is elastically recovered before the next deformation step begins. Nemat-Nasser et al. [54] confirmed that a steel sample deformed up to about 28% strain at room temperature, unloaded, cooled down to lower temperatures and deformed again up to a strain equal to 52% reached the same stress levels of a sample directly deformed up to 52% in one step at the lowest temperature. If a similar behavior is assumed for the investigated steels in this work, the JC model would successfully predict the flow behavior of austenite even though there are temperature changes.

The validity of the above approach to predict the double hit behavior was confirmed by using the data from the experiment in which $T_{def} =$ 520 °C, as no strengthening was detected for this condition. From Fig. 5a it can be concluded that the model accurately fits the results obtained at the MT, i.e. 520 °C, at which no phase formation was expected. In addition to this, the predicted YS_{Tiso} matches the YS_{Tiso} estimated by these treatments, as can be seen in Table 3. The obtained results are also in good agreement with the results obtained by Nasser et al. [54], further confirming that only the second deformation temperature and the applied plastic strain affect the yield strength, i.e. applying 10% deformation at 520 °C and then cool down to 350 °C leads to a similar yield strength than deforming up to 10% at 350 °C, if no strain induced phase transformation occurs.

When austenite is firstly deformed at 400 °C, a significant work hardening can be observed during the second deformation step, (see Fig. 5b), which indicates that a phase transformation is taking place during cooling and/or the second deformation step [37,44–48]. Under these conditions, the obtained experimental output includes a combination of the characteristics of austenite and other phases that have formed during the experiment. For that reason, the estimated yield strength is much higher than the predicted one, as reported in Table 3.

3.2.2. Extrapolation of methodology for 02C2Si and 477 L steels

Once the targeted YS_{Tiso} has been achieved, the methodology must be repeated for the remaining steels. Single hit tests, as indicated in Fig. 1b, were performed in the 02C2Si and the 477 L steels to obtain their stress-strain curves at the corresponding T_{def} and the results can be found in Fig. 6a and b. The JC model was fitted for the curve obtained at the highest temperature in both steels, in which no deviation was observed. The comparison of the experimental stress – plastic strain curves and the ones obtained by the JC model can be found in Fig. 6, where it can be observed that, at the lowest temperature in both steels, the transformation seems to start at the initial stages of the plastic regime.

Table 4
Johnson-Cook model parameters for each steel.

Steel	*A* /MPa	*B* /MPa	*m*	*n*	T_r /°C	T_m /°C
02C2Si	215.7	2650	0.8	0.80	25	1478
477 L	291.1	3899	1.0	0.82		1497
04C3SI	282.4	3407	1.0	0.89		

Regarding the use of the JC model for the double hit experiments, see Fig. 1c, the model was validated for every MT case, by using random values of ε, so it was assumed it would also work for the LT case if no strain induced transformation took place. Thus, by applying the model, the values of ε needed to achieve the corresponding YS_{Tiso} were calculated. Whereas these strains to apply can be found in Table 3, the prediction given by the JC model can be found in Fig. 5c and d. As can be seen in Table 3, the values predicted for the MT ausforming are rather close to the experimental value, thus validating the model, while the estimated yield strengths for lowest temperatures LT ausforming are much higher than expected.

3.2.3. Estimation of the driving force decrease due to the introduction of dislocations

As previously explained, plastically deforming austenite adds a new driving force to consider, ΔG_{disl}. The values of ΔG_{disl} can be calculated by Eq. (8) [40–42], where ν is the Poisson ratio and has been taken as 0.27, ρ_0 and ρ are the dislocation densities at the yield point, i.e. before any plastic deformation has been applied, and after the deformation has been applied and b_T and μ_T are the Burgers vector and the shear modulus of austenite and the corresponding temperature T_{def}.

$$\Delta G_{disl} = \frac{\mu_T b_T \left(\rho^{\frac{1}{2}} - \rho_0^{\frac{1}{2}}\right)}{8\pi(1-\nu)} \tag{8}$$

Whereas the initial dislocation density has been assumed to be $\rho_0 = 10^{11}\ m^{-2}$ [55], the final dislocation ρ can be calculated by Taylor's equation – Eq. (9)-, where $K = 0.3$ is a constant and $M = 3$ is the Taylor orientation factor [43].

$$\sigma max\ (Tdef) = YSTdef - bef + K\ M\ \mu_T\ b_T\ \sqrt{\rho} \tag{9}$$

Concerning μ_T and b_T, they can be calculated by Eqs. (10,11), respectively, where $\mu_0 = 8.1\ 10^{10}\ J\ m^{-3}$, $\left(\frac{T_m}{\mu_0}\right)\left(\frac{d\mu_T}{dT_{def}}\right) = 0.91$ and $b_0 = 2.5\ 10^{-10}$ m [56]. *TEC* stands for thermal expansion coefficient of austenite ($TEC = 2.07\ 10^{-5}\ °C^{-1}$ [57]).

$$\mu_T = \mu_0\left[1 + \left(\frac{T_{def} - 300}{T_m}\right)\left(\frac{T_m}{\mu_0}\right)\left(\frac{d\mu_T}{dT_{def}}\right)\right] \tag{10}$$

$$b_T = b_0(1 + TEC\ T_{def}) \tag{11}$$

The result of ΔG_{disl} must be converted from Pa to J mol^{-1} by multiplying it by the molar volume at each temperature as explained somewhere else [20]. The obtained values of ΔG_{disl}, besides the values of σ_{max} and ρ, are included in Table 3. It can be said that they are similar, especially in the case of the medium temperature treatments.

3.2.4. Further considerations

Finally, some further information should be added. First, previous simulation results have shown that low strains (lower than 20%) do not affect significantly affect the PAGS [58]. Therefore, it can be assumed that the PAGS are still similar for all ausforming conditions even though samples were deformed. Second, the increase of nucleation sites due to ausforming should be similar for all steels (considering the MT and LT ausforming treatments separately), because PAGS are similar and the dislocations densities are of the same order of magnitude ($10^{14}\ m^{-2}$), see Table 3. Third and last, giving the relevance that it might have on the interpretation of the forthcoming results, it was deemed as necessary to anticipate which type of phase was induced by strain during the deformation steps. Thus, the critical temperatures describing the ranges in which martensitic and bainitic transformations can occur in the presence of stress or strain (Ms(σ), Md*, Bs(σ) and Bd*) were calculated as thoroughly explained in Ref [37]. While the Ms.(σ) and Bs(σ) delimit the stress induced martensitic and bainitic transformations, respectively, the Md* and the Bd* temperatures are the ones above which no strain induced martensitic/bainitic transformations occurs after applying a true plastic strain $\varepsilon_{T\text{-}P\text{-}MAX}$ (equal to 35% in this work).

The mentioned critical temperatures are included in Table 2. As can be observed, only the upper limit of the Bd* temperatures of the steels 02C2Si and 477 L are given, as only its growth can be studied. The effect of plastic deformation on the bainitic nucleation, which is the most limiting condition for these steels, is not studied in the literature [37]. According to these calculations, the selected deformation temperatures are above Md* so martensite stress or strain induced transformations are avoided. However, all T_{def} are inevitably in the range where bainite can be stress or strain induced. Note that the formation of bainite is not fast enough to happen during the elastic regime under continuous straining, meaning that bainite is most likely strain induced [37].

4. Results and discussion

4.1. Results on pure isothermal and ausforming treatments

Dilatometry curves obtained during the isothermal holding in all the studied steels reached a steady state, see Fig. 7, indicating that the transformation had been completed after less than 1 h. The 04C3Si steel was shown to be the fastest one, followed by the 02C2Si steel and the 477 L steel, respectively. For some ausforming treatments, the longitudinal change in length was shown to decrease with respect to time. For the 02C3Si and 04C3Si steels subjected to LT and MT ausforming, it only occurred during the first 125 and 200 s, respectively. However, for the 04C3Si and 477 L steels subjected to LT ausforming, this behavior was kept for the entire holding. Such an effect has been observed in other ausforming treatments in which anisotropic microstructures were found [29].

Martensitic transformation was not detected on cooling to room temperature for the 04C3Si and 477 L steels, whereas it was detected for the 02C2Si steel in all treatments. Martensite formation occurs when, once the T_0 curve is reached, the associated carbon enrichment is still not high enough for the austenite to be stable at room temperature. For the 02C2Si steel, the martensite volume fraction, $V_{\alpha'}$, was quantified from the dilatometry curve by applying the level rule [22,59,60] and the estimated fractions of martensite are included in Table 5, being all of them lower than 7%.

Fig. 8-9 show the microstructures obtained after the pure isothermal, MT and LT ausforming treatments, respectively. Apart from the mentioned fresh martensite, the microstructures are composed of bainitic ferrite and austenite, see Table 5 for volume fractions of those phases ($V_{\alpha B}$ and V_γ, respectively). Note that $V_{\alpha B}$ was obtained by subtracting $V_{\alpha'}$ from the ferrite volume fraction obtained by XRD. Regarding the bainitic ferrite morphology, it can be seen that, while it is always plate-like in the microstructures obtained by pure isothermal treatments, see Fig. 8, this morphology is only observed for the two medium carbon steels subjected to ausforming treatments, whereas the microstructure obtained by ausforming in the 02C2Si steel consists of granular bainite with some plate-like bainitic areas, see Fig. 9a and d and Fig. 10a and d. Concerning a possible anisotropic growth, an alignment of the bainitic ferrite plates was observed for the low temperature ausforming performed to the 04C3Si steel, phenomenon characteristic of anisotropic transformations, in good agreement with the dilatometric results [29]. This alignment is also slightly present in some regions of the sample corresponding to MT ausforming performed on the 02C2Si steel,

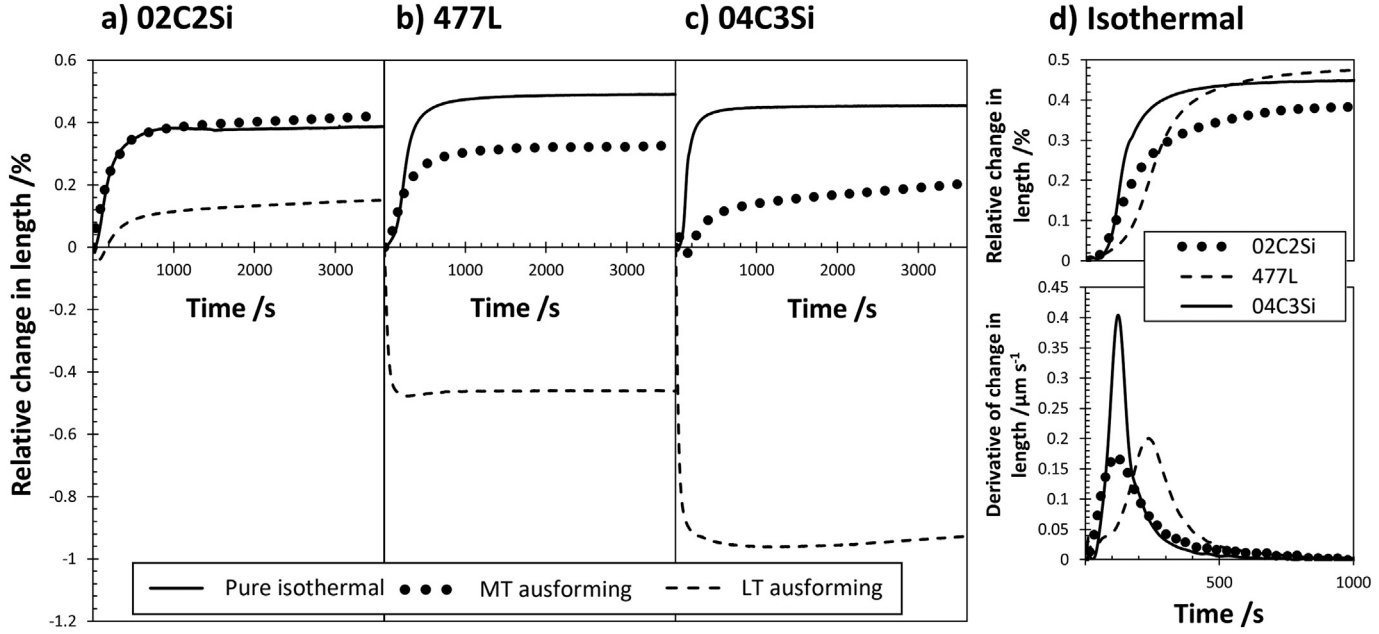

Fig. 7. Relative change in length vs. time plots obtained by treatments in Fig. 1a for the steels a) 02C2Si; b) 477 L and c) 04C3Si. where MT and LT stand for medium and low temperature, respectively. d) Detail of the relative change in length vs. time plot and derivative of change in length vs. time plot corresponding to the pure isothermal treatments.

although it was not found in the sample where LT ausforming was carried out on the same steel. Such effects are not so evident for the 477 L steel, even though dilatometry suggests otherwise.

The microstructures also differ from each other in terms of austenite block sizes, i.e. the size of the blocks of austenite which are located in between bainitic sheaves. While the microstructures obtained in the 04C3Si steel only have sub-micron blocks, the rest of the other steels have many coarser blocks homogeneously distributed along the microstructure.

Plate thicknesses have been measured as described in Section 2 and their corresponding average plate thicknesses can be found in Table 5. Note that, for the 02C2Si steel, granular bainite areas have not been considered as the stereology used in Ref. [19] only applies for plate-like features. Fresh martensite could not be distinguished from bainitic ferrite in the 02C2Si samples and, although its fraction was low, it might have slightly influenced the plate thickness measurements. Note that martensite plates or laths are usually from 200 to 500 nm thick [61].

First of all, the pure isothermal conditions were studied. Although all microstructures are plate-like, the microstructure obtained in the 04C3Si steel is the most refined one, whereas the remaining steels microstructures are coarser. As the isothermal temperatures were selected so that $\Delta G_{chem}^{\gamma\rightarrow\alpha}$ is the same for all steels and those temperatures are all close to each other, see Table 3. The only parameter that differs from one sample to the other is YS_{Tiso}. When comparing the results of the 477 L and the 04C3Si steels, see Table 5, it is evident that the plate thickness differences cannot be explained based on the parameters of the current theory, as both steels have comparable T_{iso} and the difference in yield strength values at the selected isothermal temperatures between both steels is only 14 MPa, as shown in Table 3.

If the variations of plate thickness are assessed from a theoretical point of view, using the model developed by Yang et al. [8], variation of the original model by Singh and Bhadeshia [5], the same conclusion is made. This model's inputs are the ones already discussed, i.e. T_{iso} (in °C), $\Delta G_{chem}^{\gamma\rightarrow\alpha}$ at the isothermal temperature (in J mol^{-1}), and YS_{Tiso} (in MPa). It reads as follows:

$$t\,[nm] = 222 + 0.01242 \cdot T_{iso} + 0.01785 \cdot \Delta G_{chem}^{\gamma\rightarrow\alpha} - 0.5323 \cdot YS_{Tiso} \qquad (4)$$

Note that this model does not consider the PAGS, even though some works have shown that it affects plate thickness, as previously explained. However, there are no holistic more complete models at this point. Results thus obtained are gathered in Table 5, where it can be seen that, while there is a reasonably good fitting for 04C3Si, for the other two steels, the experimental plate thicknesses are about twice

Table 5
Data regarding all treatments, where T_{iso} and T_{def} stand for isothermal temperature and deformation temperature, respectively, ε is the applied strain. The volume fractions of the different phases: martensite ($V_{\alpha'}$), bainitic ferrite ($V_{\alpha B}$) and austenite (V_{γ}), besides the plate thicknesses, measured on the transverse and the longitudinal sections, t_T and t_L, the predicted t (PrEd.), the austenite carbon content, C_{γ}, and the Vickers hardness (load of 10 kg, HV10).

Steel	T_{iso} /°C	T_{def} /°C	ε /%	$V_{\alpha'}$ (±1) /%	$V_{\alpha B}$ (±3) /%	V_{γ} (±3) /%	t_T / nm	t_L /nm	Pred. t/nm	C_{γ} (±0.06) /wt%	HV10
02C2Si	367	–	–	3	87	10	219 ± 9	226 ± 7	121	0.80	407 ± 3
		530	16.0	7	77	16	236 ± 6	245 ± 8	–	0.63	404 ± 5
		410	20.0	2	88	10	218 ± 9	234 ± 9	–	0.74	403 ± 5
477 L	342	–	–	–	82	18	170 ± 5	187 ± 5	90	0.92	466 ± 2
		512	8.5	–	81	19	171 ± 5	173 ± 5	–	0.85	479 ± 5
		392	10.5	–	80	20	252 ± 6	244 ± 6	–	0.97	475 ± 5
04C3Si	350	–	–	–	79	21	82 ± 2	93 ± 3	80	1.07	485 ± 2
		520	10.0	–	76	24	101 ± 3	103 ± 3	–	1.04	489 ± 5
		400	10.0	–	73	27	102 ± 3	96 ± 2	–	1.24	487 ± 1

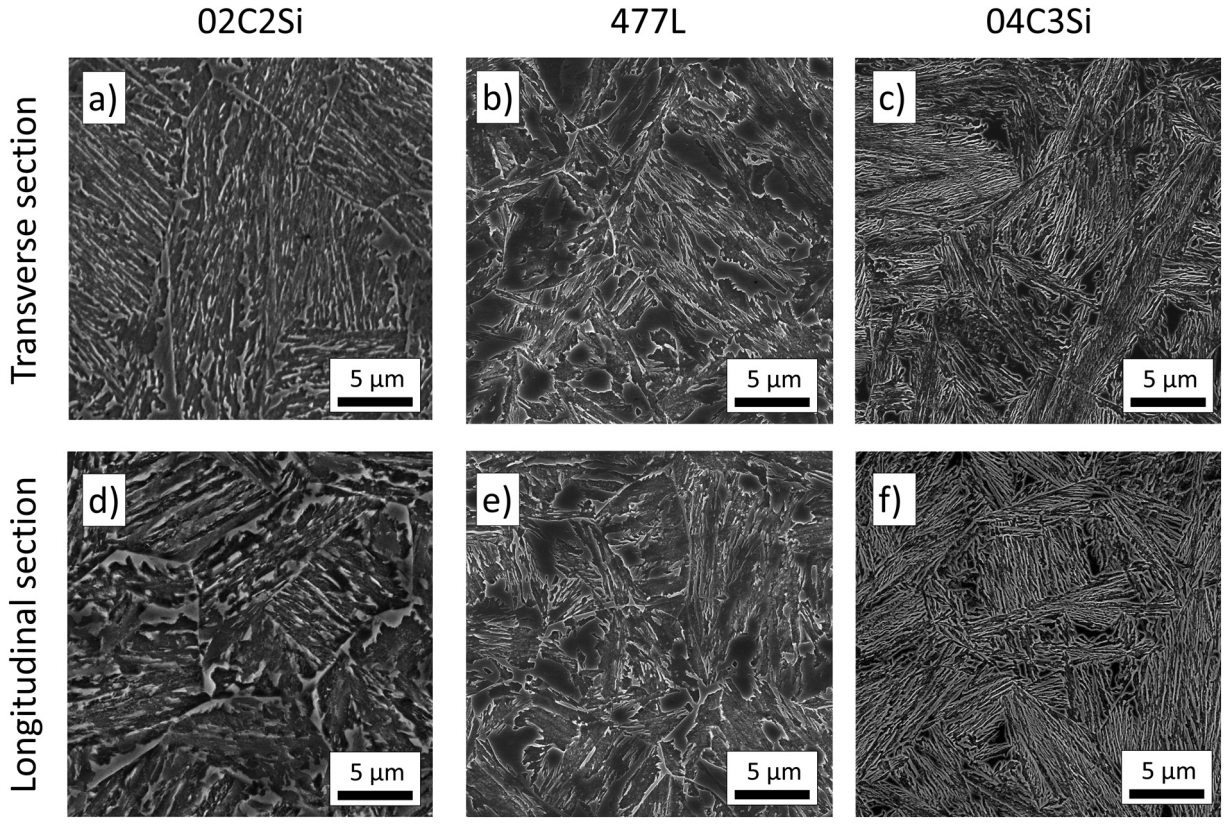

Fig. 8. Microstructures obtained after isothermally treating the samples at the corresponding T_{iso}, where a), b) and c) show the transverse sections, whereas d), e) and f) show the longitudinal sections of the 02C2Si, 477 L and 04C3Si respectively.

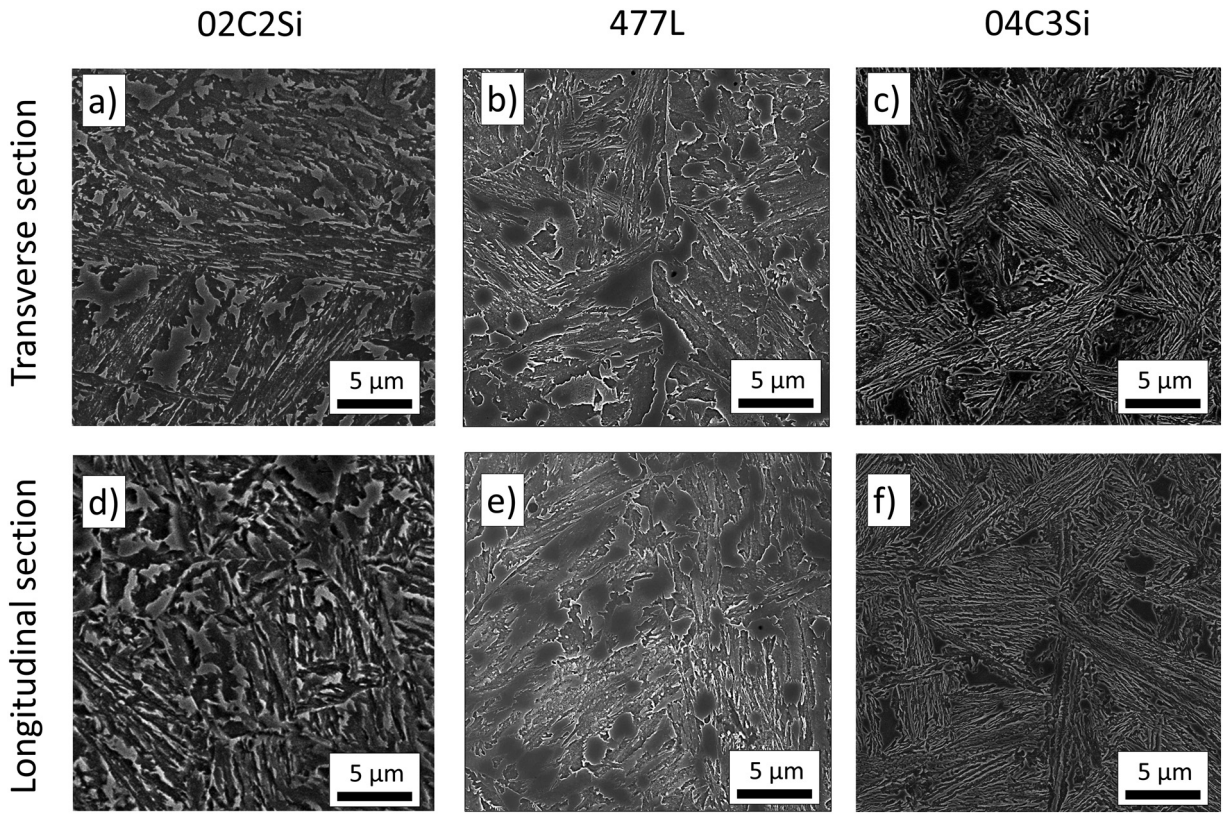

Fig. 9. Microstructures obtained after the medium temperature (MT) ausforming treatments, where a), b) and c) show the transverse sections, whereas d), e) and f) show the longitudinal sections of the 02C2Si, 477 L and 04C3Si respectively. The deformation - 16% (a,d); 8.5% (b,e) and 10% (c,f) - has been applied vertically.

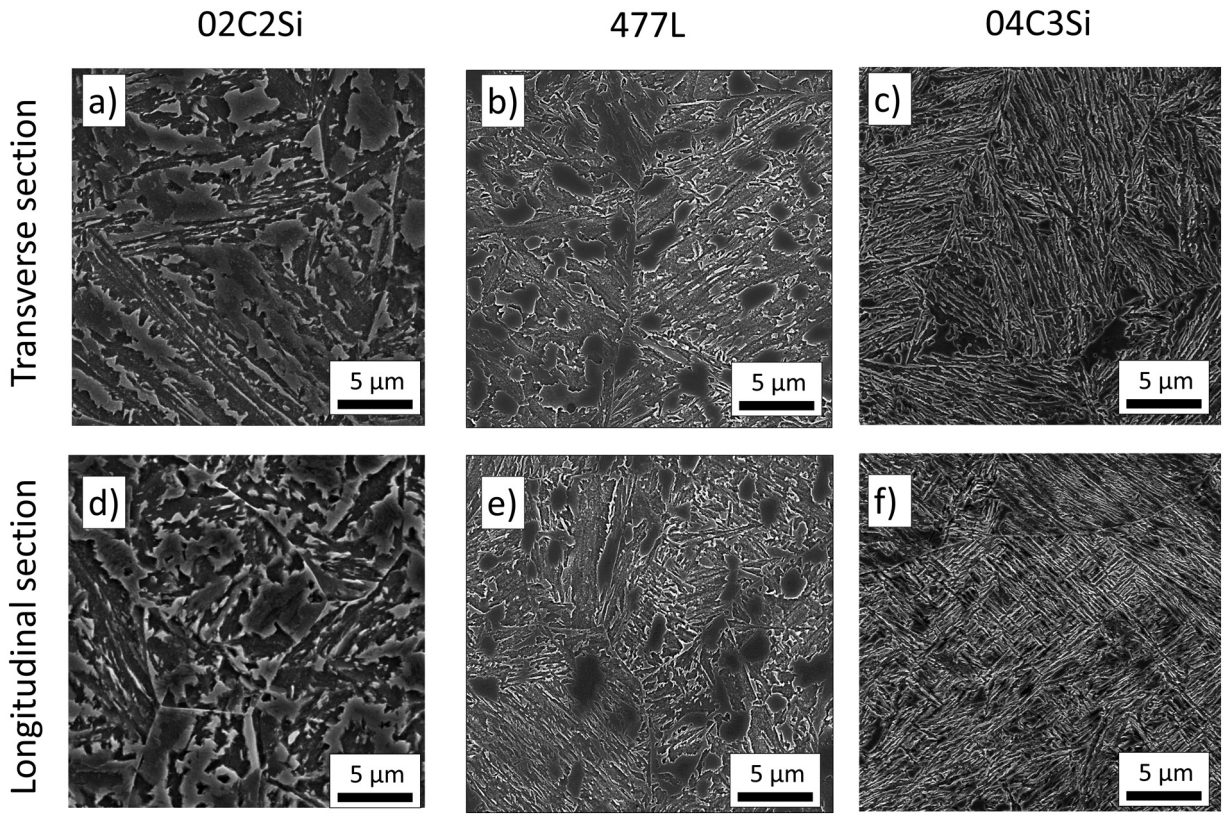

Fig. 10. Microstructures obtained after the low temperature (LT) ausforming treatments, where a), b) and c) show the transverse sections, whereas d), e) and f) show the longitudinal sections of the 02C2Si, 477 L and 04C3Si respectively. The deformation - 20% (a,d); 10.5% (b,e) and 10% (c,f) - has been applied vertically.

the predicted ones, meaning that the model is not taking into account one or several factors which are rather influent for those two steels.

When it comes to the ausforming treatments, it is evident that applying the current theory was not enough to obtain similarly refined microstructures. As can be observed, the average plate thickness values do not vary significantly when applying ausforming. Additionally, a significant coarsening is detected in the LT ausforming sample of the 477 L steel, most likely due to the strain induced formation of bainite during the compression step, as anticipated above. Although the comparison of the JC stress strain curves with the experimental curves performed in section 3.2.2 suggest that the 02C2Si steel subjected to LT ausforming also presented strain induced transformations, it is possible that the formed strain induced bainite is granular bainite, which was been included in these measurements. Note that, for the 04C3Si steel, no strain induced transformations were detected by the comparison of the JC stress strain curve with the experimental curve at 400 °C for a 10% strain (they were detected for strains higher than 12%) and, although a previous study has shown that for that stage some strain induced transformation had already started, it can be assumed that its fraction was rather low and the average plate thickness was barely changed by it [37].

Regarding the hardness values, in the case of the pure isothermal treatments, it is clear that they mainly depend on the plate thickness, as previously reported [62]. For the ausforming treatments, the strengthening due to plastic deformation and (only for the 02C2Si steel) the presence of fresh martensite seem to compensate the strength loss because of the increase of austenite volume fraction and the plates coarsening, see Table 5, as the hardness values are very similar for all conditions in every steel regardless of which thermal and thermomechanical treatment had been applied.

At this point, the representation of the line intercept histograms provides a valuable insight on the understanding of the topic of research of this work. Fig. 11 includes box and whisker plots of the line intercepts measured on SEM micrographs of the pure isothermal and the MT ausforming samples. The histograms of the LT ausforming treatments were not represented as they were altered by strain induced bainitic transformations. These plots enable to obtain extensive information about statistical data, such as the lower and upper quartiles, Q_1 and Q_3, respectively, which are represented by a box, the median, Q_2., drawn as a line crossing through the box, the fifth and ninety-fifth percentiles, P_5 and P_{95}, illustrated by filled diamonds and the mean value, depicted by filled squares. The end of the whisker marks off the lowest datum within 1.5 times IQR ($IQR = Q_3 - Q_1$) below Q_1 and the highest datum within 1.5 times IQR above Q_3.

In the analysis of the above data, it must be noted that, while the 477 L and the 02C2Si line intercepts histograms point to a normal distribution behavior, the distribution looks to be less mean-centered, as in a lognormal distribution, in the case of 04C3Si. Also, the largest interquartile range ($IQR = Q_3 - Q_1$) is found for the 02C2Si steel, followed by the one for the 477 L and the 04C3Si steels. Note that, under the assumption of isotropy, the IQR should be constant for any fixed plate thickness, as it would only depend on stereology. Different IQR values mean that the plate thickness values are more scattered, most likely because the plate thickness evolves throughout the transformation and because this evolution was not identical for all steels.

4.2. Dynamic changes of the system as the transformation progresses

At this point, and with the theory and tools at hand, we must note that, so far, the parameters considered to study the scale of bainitic microstructures have been calculated based on the chemical composition of the bulk. In other words, the whole system has been considered static throughout the transformation. However, the system has been proved to evolve as the transformation advances. It is worth noting that most

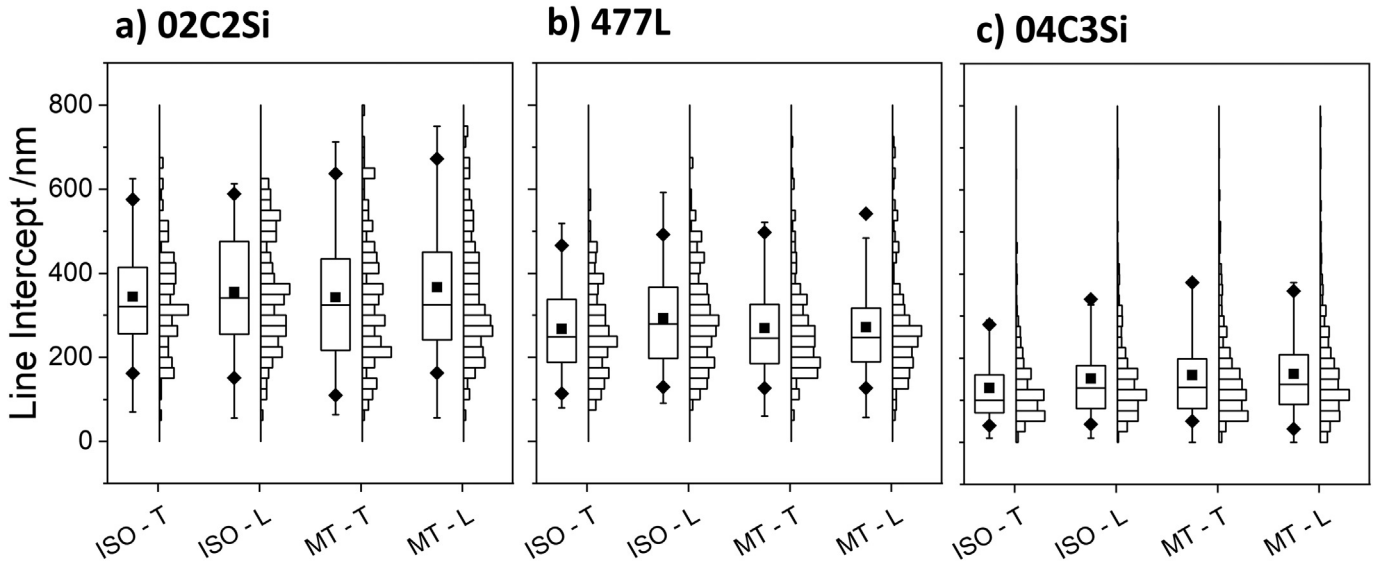

Fig. 11. Box and whisker plots representing the line intercepts dataset measured from the transverse (T) and longitudinal (L) sections of the microstructures obtained by pure isothermal (ISO) and medium temperature ausforming (MT) treatments in a) steel 02C2Si; b) steel 477 L and c) steel 04C3Si. The boxes are delimited by the lower and upper quartiles, Q_1 and Q_3, respectively, the line crossing through them is the data median, Q_2. The end of the whisker marks off the lowest datum within 1.5 times IQR below Q_1 and the highest datum within 1.5 times IQR above Q_3. The fifth and ninety-fifth percentiles, P_5 and P_{95}, are illustrated by filled diamonds, whereas the mean value is represented by a filled square.

of the works published so far on the topic deal with such evolution by comparison of the beginning and end of the transformation, but not its actual evolution as the transformation progresses [8,18].

In an attempt to put some light in this matter, the following paragraphs depict how some of those parameters evolve during the transformation, and how their evolution might affect the final scale of the microstructure.

To begin with, we should consider the evolution of austenite carbon content and the dislocation density, which increases as the degree of transformation increases. First of all, as generally agreed, bainite sheaves usually nucleate at the austenite grain boundaries and then propagate toward the grain center by a stress-induced autocatalytic phenomenon, i.e. individual ferrite plates nucleate at the surface of previously formed ones, not triggered by strain but by stress [10]. As the transformation goes on, both, the austenite dislocation density and the austenite carbon content increase [10,63,64], although they do not increase homogeneously along the retained austenite. The dislocations created to plastically accommodate the transformation strain in austenite are accumulated near the ferrite/austenite interphase [65–68], where the austenite carbon enrichment is also more pronounced [69–74]. Therefore, the austenite surrounding a just-grown plate is modified in several ways: a) the local driving force in that area is decreased (in absolute value) because of the carbon enrichment, making the transformation less likely to happen. However, because of the introduced stress state, more plates are stimulated to grow and b) the local austenite yield strength – note that he word "local" is used so that the term is not mistaken for the "global" yield strength of the microstructure, which would be an average along the whole specimen - is increased as the local dislocation density and the local carbon content in that region do, which in principle should imply a refinement of the subsequent bainitic ferrite plates. Note that, as a result of the increase in the local yield strength of austenite, the interface of the next plate to grow will have to exert more tension to advance and overcome it, and again, it is likely that the advancing interface generates even more dislocations than in previous stages, which in turn affects the next growing plates. The concept of a dynamic system in continuous change as the bainitic transformation proceeds has been also introduced by van Bohemen [64] when explaining why bainitic transformation is so sluggish in the latest stages.

Therefore, the C content of austenite, far from remaining static, evolves from that of the bulk (right before transformation starts) to that given by the T_0 curve (end of transformation) [71,75] and, as already mentioned, this modifies the austenite strength and the driving force for the transformation, with the consequent plate thickness variation as the transformation progresses.

In this regard, it is possible to calculate the maximum C enrichment of the retained austenite by correlating its lattice parameter with its chemical composition by means of Dyson and Holmes [26] formulation. As shown in Table 5, the 04C3Si steel, which shows the finest bainitic ferrite plates, presents the highest enrichment level (C_γ-C_{bulk}, where C_{bulk} is the carbon content of the bulk steel), in between 0.61 and 0.81 $\pm$ 0.03 wt%, as compared to the 477 L, with a C-enrichment of 0.45–0.57 $\pm$ 0.03 wt%. Note that, in the case of 02C2Si steel, in which martensite formation was detected on cooling to room temperature, the C-enrichment at T_{ISO} should be smaller than the one obtained by XRD, which is 0.43–0.60 $\pm$ 0.03 wt%. The C-enrichment differences are due to the different solute contents in the steels, which modify the T_0 curve [76–78].

Another factor to consider is that a high growth rate is equivalent to a high strain rate, which not only makes yielding more difficult but also increases the impingements events, again affecting the plate thickness [10]. In this regard, Fig. 7d clearly shows that the transformation kinetic of the 04C3Si steels is far faster than that of 02C2Si and 477 L, in decreasing order. If we also consider that the above-mentioned C enrichment of austenite is superior in the former, and it is attained in a much faster fashion than the later, we could find a lead to explain the differences found in the plate thickness and its distribution. Note that the incubation times, shorter in the cases of the 04C3Si and 02C2Si steels, do not affect the transformation in this matter.

This work demonstrates that the physical mechanisms laying behind the effect of these parameters on the final microstructure need to be clarified. This requires other tools and an independent research that considers the dynamic character of the system as the transformation progresses in order to promote the design of new steel grades with improved properties.

5. Conclusion

In this work, ausforming treatments were designed to obtain the same bainitic plates thicknesses by means of yield strength and driving force for the transformation, according to the literature. However, the application of ausforming was not successful, because of two factors: (1) the deformation seems to have promoted strain induced bainitic transformations, especially at low temperatures; the presence of such phase alters the average plate thickness; and (2) even for the ausforming treatments in which no strain induced transformations occurred, the plate did not have the same scale, showing that there may be other parameters but the ones studied in the literature that influence the bainitic ferrite plate thickness.

The analysis of the line intercepts data indicates that the variability of the plate thickness is different for the three steels, suggesting that the evolution of the local austenite conditions could play a role in the final microstructure scale. Based on the kinetics of the transformation and on the carbon content of austenite at the end of the transformation, a possible explanation has been proposed to explain the different scales of the microstructures.

Author contributions

Conceptualization: AEC, CGM; Investigation: AEC, JH, MZ, ITC; Supervision: MJ, FGC and CGM; Writing original draft: AEC and CGM; Writing: AEC, JH, MZ, MJ, ITC, FGC and CGM.

Declaration of Competing Interest

The authors declare that they have no known competing financial interests or personal relationships that could have appeared to influence the work reported in this paper.

Acknowledgements

Richard Huizenga at the Department of Materials Science and Engineering of the Delft University of Technology is acknowledged for the X-ray analysis. The authors gratefully acknowledge the support for this work by the European Research Fund for Coal and Steel under the Contracts RFCS-2015-709607 & RFCS-2019-899482 and by the Program Atracción de talento investigador (Consejería de Educación, Juventud y Deporte, Comunidad de Madrid), under the fellowship 2016-T2/IND-1693. They also acknowledge the support provided by the subsequent laboratories belonging to CENIM: X-Ray Diffraction, Metallography and Phase Transformations. The financial and equipment support from National Science and Engineering Research Council (NSERC) Canada is acknowledged by M. Jahazi and M. Zorgani acknowledges the scholarship provided by the Lybian government for his PhD studies.

References

[1] F.G. Caballero, H.K.D.H. Bhadeshia, K.J.A. Mawella, D.G. Jones, P. Brown, Very strong low temperature bainite, Mater. Sci. Technol. 18 (2002) 279–284.
[2] C. Garcia-Mateo, F.G. Caballero, Ultra-high-strength bainitic steels, ISIJ Int. 45 (2005) 1736–1740.
[3] C. Garcia-Mateo, F.G. Caballero, T. Sourmail, M. Kuntz, J. Cornide, V. Smanio, et al., Tensile behaviour of a nanocrystalline bainitic steel containing 3wt% percent silicon, Mater. Sci. Eng. A 549 (2012) 185–192.
[4] T. Sourmail, V. Smanio, C. Ziegler, V. Heuer, M. Kuntz, F.G. Caballero, et al., Novel Nanostructured Bainitic Steel Grades to Answer the Need for High-Performance Steel Components (Nanobain).RFSR-CT-2008-00022, Luxembourg, European Commission, 2013.
[5] S.B. Singh, H.K.D.H. Bhadeshia, Estimation of bainite plate-thickness in low-alloy steels, Mater. Sci. Eng. A 245 (1998) 72–79.
[6] J. Cornide, C. Garcia-Mateo, C. Capdevila, F.G. Caballero, An assessment of the contributing factors to the nanoscale structural refinement of advanced bainitic steels, J. Alloys Compd. 577 (2013) S43-S7.
[7] C. Garcia-Mateo, G. Paul, M.C. Somani, D.A. Porter, L. Bracke, A. Latz, et al., Transferring Nanoscale Bainite concept to lower C contents: A perspective, Metals. 7 (2017) 159.
[8] Z. Yang, C. Chu, F. Jiang, Y. Qin, X. Long, S. Wang, et al., Accelerating nano-bainite transformation based on a new constructed microstructural predicting model, Mater. Sci. Eng. A 748 (2019) 16–20.
[9] E. Swallow, H.K.D.H. Bhadeshia, High resolution observations of displacements caused by bainitic transformation, Mater. Sci. Technol. 12 (1996) 121–125.
[10] H.K.D.H. Bhadeshia, Bainite in Steels: Theory and Practice, 3 ed Maney Publishing, 2015.
[11] M. Kabirmohammadi, B. Avishan, S. Yazdani, Transformation kinetics and microstructural features in low-temperature bainite after ausforming process, Mater. Chem. Phys. 184 (2016) 306–317.
[12] M. Zhang, Y. Wang, C. Zheng, F. Zhang, T. Wang, Effects of ausforming on isothermal bainite transformation behaviour and microstructural refinement in medium-carbon Si–Al-rich alloy steel, Mater. Des. 62 (2014) 168–174.
[13] L.C. Chang, H.K.D.H. Bhadeshia, Metallographic observations of Bainite transformation mechanism, Mater. Sci. Technol. 11 (1995) 105–108.
[14] L. Lan, C. Qiu, D. Zhao, X. Gao, L. Du, Effect of austenite grain size on isothermal bainite transformation in low carbon microalloyed steel, Mater. Sci. Technol. 27 (2011) 1657–1663.
[15] K. Singh, A. Kumar, A. Singh, Effect of prior austenite grain size on the morphology of Nano-Bainitic steels, Metall Mater Trans A. 49 (2018) 1348–1354.
[16] T. Jiang, H. Liu, J. Sun, S. Guo, Y. Liu, Effect of austenite grain size on transformation of nanobainite and its mechanical properties, Mater. Sci. Eng. A 666 (2016) 207–213.
[17] C. Garcia-Mateo, FG C, HKDH B., Acceleration of low-temperature bainite, ISIJ Int. 43 (2003) 1821–1825.
[18] M. Azuma, N. Fujita, M. Takahashi, T. Senuma, D. Quidort, T. Lung, Modelling upper and lower bainite trasformation in steels, ISIJ Int. 45 (2005) 221–228.
[19] C. Garcia-Mateo, J.A. Jimenez, B. Lopez-Ezquerra, R. Rementeria, L. Morales-Rivas, M. Kuntz, et al., Analyzing the scale of the bainitic ferrite plates by XRD, SEM and TEM. Mater Charact. 122 (2016) 83–89.
[20] A. Eres-Castellanos, I. Toda-Caraballo, A. Latz, F.G. Caballero, C. Garcia-Mateo, An integrated-model for austenite yield strength considering the influence of temperature and strain rate in lean steels, Mater. Des. 108435 (2019).
[21] T. Sourmail, V. Smanio, Low temperature kinetics of bainite formation in high carbon steels, Acta Mater. 61 (2013) 2639–2648.
[22] H.S. Yang, H.K.D.H. Bhadeshia, Uncertainties in dilatometric determination of martensite start temperature, Mater. Sci. Technol. 23 (2007) 556–560.
[23] C.F. Jatczak, Retained austenite and its measurement by X-ray diffraction, SAE Trans. (1980) 1657–1676.
[24] M.J. Dickson, Significance of texture parameters in phase analysis by X-ray diffraction, J. Appl. Crystallogr. 2 (1969) 176–180.
[25] R.A. Young, The Rietveld Method: International Union of Crystallography, 1993.
[26] D.J. Dyson, B. Holmes, Effect of alloying additions on lattice parameter of austenite, J Iron Steel Inst. 208 (1970) 469–474.
[27] A. Shirzadi, H. Abreu, L. Pocock, D. Klobčuar, P. Withers, H. Bhadeshia, Bainite orientation in plastically deformed austenite, Int. J. Mater. Res. 100 (2009) 40–45.
[28] Fan H-l, Zhao A-m, Li Q-c, H. Guo, J.-G. He, Effects of ausforming strain on bainite transformation in nanostructured bainite steel, International Journal of Minerals, Metallurgy, and Materials 24 (2017) 264–270.
[29] A. Eres-Castellanos, L. Morales-Rivas, A. Latz, F.G. Caballero, C. Garcia-Mateo, Effect of ausforming on the anisotropy of low temperature bainitic transformation, Mater. Charact. 145 (2018) 371–380.
[30] C.G. de Andres, F.G. Caballero, C. Capdevila, Martin D. San, Revealing austenite grain boundaries by thermal etching: advantages and disadvantages, Mater. Charact. 49 (2002) 121–127.
[31] W. Rasband, ImageJ, US National Institutes of Health, Bethesda, MD, 1997.
[32] Laboratory NP. MTDATA: Phase Diagram Calculation Software. Teddington, Middlesex, UK, TW11 0LW2004.
[33] C. Garcia-Mateo, H.K.D.H. Bhadeshia, Nucleation theory for high-carbon bainite, Mater. Sci. Eng. A 378 (2004) 289–292.
[34] H. Bhadeshia, A rationalisation of shear transformations in steels, Acta Metall. 29 (1981) 1117–1130.
[35] H. Bhadeshia, A. Waugh, Bainite: an atom-probe study of the incomplete reaction phenomenon, Acta Metall. 30 (1982) 775–784.
[36] G. Ghosh, G.B. Olson, Kinetics of FCC→ BCC heterogeneous martensitic nucleation—I. the critical driving force for athermal nucleation, Acta Metall. Mater. 42 (1994) 3361–3370.
[37] A. Eres-Castellanos, F.G. Caballero, C. Garcia-Mateo, Stress or strain induced martensitic and Bainitic transformations during ausforming processes, Acta Mater. 189 (2020) 60–72.
[38] A.M. Ravi, A. Kumar, M. Herbig, J. Sietsma, Santofimia MJ, Impact of austenite grain boundaries and ferrite nucleation on bainite formation in steels, Acta Materialia, 2020.
[39] W. Gong, Y. Tomota, M.S. Koo, Y. Adachi, Effect of ausforming on nanobainite steel, Scr. Mater. 63 (2010) 819–822.
[40] M. Maalekian, E. Kozeschnik, S. Chatterjee, H.K.D.H. Bhadeshia, Mechanical stabilisation of eutectoid steel, Mater. Sci. Technol. 23 (2007) 610–612.
[41] S. Chatterjee, H.S. Wang, J.R. Yang, H.K.D.H. Bhadeshia, Mechanical stabilisation of austenite, Mater. Sci. Technol. 22 (2006) 641–644.
[42] H.K.D.H. Bhadeshia, R.W.K. Honeycombe, Steels: Microstructure and Properties: Butterworths-Heinemann, Elsevier, 2006.
[43] G.I. Taylor, The mechanism of plastic deformation of crystals. Part I.—Theoretical, Proceedings of the Royal Society of London Series A, Containing Papers of a Mathematical and Physical Character, 145, 1934, pp. 362–387.
[44] G.C. Soares, M.C.M. Rodrigues, LdA Santos, Influence of temperature on mechanical properties, fracture morphology and strain hardening behavior of a 304 stainless steel, Mater. Res. 20 (2017) 141–151.

[45] J. Talonen, H. Hänninen, P. Nenonen, G. Pape, Effect of strain rate on the strain-induced γ→ α'-martensite transformation and mechanical properties of austenitic stainless steels, Metall. Mater. Trans. A 36 (2005) 421–432.
[46] X. Fang, W. Dahl, Strain hardening and transformation mechanism of deformation-induced martensite transformation in metastable austenitic stainless steels, Mater. Sci. Eng. A 141 (1991) 189–198.
[47] X. Fang, C. Gusek, W. Dahl, Strain hardening of steels at large strain deformation. Part II: strain hardening of pearlitic and austenitic steels and the estimation of mechanical properties, Mater. Sci. Eng. A 203 (1995) 26–35.
[48] S. Lin, Deformation-Induced Martensitic Transformation and Mechanical Properties of Duplex and Austenitic Stainless Steels: A Synchrotron X-Ray Diffraction Study, 2017.
[49] G.R. Johnson, A constitutive model and data for materials subjected to large strains, high strain rates, and high temperatures, Proc 7th Inf Sympo Ballistics 1983, pp. 541–547.
[50] L. Schwer, Optional Strain-rate forms for the Johnson Cook Constitutive Model and the Role of the parameter Epsilon_0. 6th European LS_DYNA Users' Conference, 2007 1–17.
[51] R. Liang, A.S. Khan, A critical review of experimental results and constitutive models for BCC and FCC metals over a wide range of strain rates and temperatures, Int. J. Plast. 15 (1999) 963–980.
[52] A. Sobolev, M. Radchenko, Use of Johnson–cook plasticity model for numerical simulations of the SNF shipping cask drop tests, Nuclear Energy and Technology. 2 (2016) 272–276.
[53] A.B. Tanner, R.D. McGinty, D.L. McDowell, Modeling temperature and strain rate history effects in OFHC cu, Int. J. Plast. 15 (1999) 575–603.
[54] S. Nemat-Nasser, W.-G. Guo, Thermomechanical response of DH-36 structural steel over a wide range of strain rates and temperatures, Mech. Mater. 35 (2003) 1023–1047.
[55] E. Galindo-Nava, A. Perlade, P. Rivera-Díaz-del-Castillo, A thermostatistical theory for solid solution effects in the hot deformation of alloys: an application to low-alloy steels, Model. Simul. Mater. Sci. Eng. 22 (2013), 015009, .
[56] Parker S. Victoria, Modelling of Phase Transformations in Hot-Rolled Steels, University of Cambridge, 1997.
[57] A. Saha Podder, H.K.D.H. Bhadeshia, Thermal stability of austenite retained in bainitic steels, Mater. Sci. Eng. A 527 (2010) 2121–2128.
[58] N. Xiao, M. Tong, Y. Lan, D. Li, Y. Li, Coupled simulation of the influence of austenite deformation on the subsequent isothermal austenite–ferrite transformation, Acta Mater. 54 (2006) 1265–1278.
[59] A. Navarro-López, J. Sietsma, M. Santofimia, Effect of prior athermal martensite on the isothermal transformation kinetics below M s in a low-C high-Si steel, Metall. Mater. Trans. A 47 (2016) 1028–1039.
[60] S. Van Bohemen, J. Sietsma, Effect of composition on kinetics of athermal martensite formation in plain carbon steels, Mater. Sci. Technol. 25 (2009) 1009–1012.
[61] E. Pereloma, D.V. Edmonds, Phase Transformations in Steels: Diffusionless Transformations, High Strength Steels, Modelling and Advanced Analytical Techniques: Elsevier, 2012.
[62] H.K.D.H. Bhadeshia, D.V. Edmonds, The mechanism of bainite formation in steels, Acta Metall. 28 (1980) 1265–1273.
[63] R.K. Dutta, R.M. Huizenga, M. Amirthalingam, M.J.M. Hermans, A. King, I.M. Richardson, Transformation-induced diffraction peak broadening during Bainitic and martensitic transformations under small external loads in a quenched and tempered high strength steel, Metall Mater Trans A. (2013) 1–4.
[64] S. van Bohemen, Bainite growth retardation due to mechanical stabilisation of austenite, Materialia. 7 (2019) 100384.
[65] S. He, B. He, K. Zhu, M. Huang, Evolution of dislocation density in bainitic steel: modeling and experiments, Acta Mater. 149 (2018) 46–56.
[66] F.C. Frank, Martensite, Acta Metall. 1 (1953) 15–21.
[67] G. Olson, M. Cohen, Interphase-boundary dislocations and the concept of coherency, Acta Metall. 27 (1979) 1907–1918.
[68] Sandvik BPJ, C.M. Wayman, Characteristics of Lath Martensite: Part I. Crystallographic and Substructural Features, Metallurgical transactions A, Physical metallurgy and materials science 14 (1983) 809–822.
[69] G.I. Rees, H.K.D.H. Bhadeshia, Bainite transformation kinetics. Part1. Modified Model, Mater science and Tech. 8 (1992) 985–993.
[70] P.G. Self, H.K.D.H. Bhadeshia, W.M. Stobbs, Lattice SPACINGS from lattice fringes, Ultramicroscopy. 6 (1981) 29–40.
[71] H.K.D.H. Bhadeshia, A.R. Waugh, Bainite: an atom-probe study of the incomplete reaction phenomenon, Acta Metall. 30 (1982) 775–784.
[72] Z. Lawrynowicz, Carbon partitioning during bainite transformation in low alloy steels, Mater. Sci. Technol. 18 (2002) 1322–1324.
[73] S.J. Matas, R.F. Hehemann, The structure of BAINITE in HYPOEUTECTOID steels, Trans Metall AIME. 221 (1961) 179–185.
[74] A. Schrader, F. Wever, Zur Frage der Eignung des Elektronenmikroskops für die Gefügeuntersuchung von Stählen, Archiv für das Eisenhüttenwesen. 23 (1952) 489–495.
[75] L.C. Chang, H.K.D.H. Bhadeshia, Carbon content of austenite in isothermally transformed 300m steel, Mater. Sci. Eng. A 184 (1994) L17-L9.
[76] H. Bhadeshia, New bainitic steels by design, Modelling and simulation for materials design. (1998) 227–232.
[77] M. Takahashi, H.K.D.H. Bhadeshia, A model for the microstructure of some advanced bainitic steels, Mater. Trans. JIM 32 (1991) 689–696.
[78] K.I. Sugimoto, N. Usui, M. Kobayashi, S.I. Hashimoto, Effects of volume fraction and stability of retained austenite on ductility of TRIP-aided dual-phase steels, ISIJ Int. 32 (1992) 1311–1318.